Solid State Communications 251 (2017) 88–93

Contents lists available at ScienceDirect

Solid State Communications

journal homepage: www.elsevier.com/locate/ssc

Fast track communication

How much does size really matter? Exploring the limits of graphene as Li ion battery anode material

H. Sun[a], A. Varzi[b,c], V. Pellegrini[a], D.A. Dinh[a,d], R. Raccichini[b,c], A.E. Del Rio-Castillo[a], M. Prato[e], M. Colombo[e], R. Cingolani[a], B. Scrosati[a], S. Passerini[b,c,*], F. Bonaccorso[a,*]

[a] Istituto Italiano di Tecnologia, Graphene Labs, I-16163 Genova, Italy
[b] Helmholtz Institute Ulm (HIU), Helmholtzstrasse 11, 89081 Ulm, Germany
[c] Karlsruhe Institute of Technology (KIT), P.O. Box 3640, 76021 Karlsruhe, Germany
[d] Università di Genova, Dipartimento di Chimica e Chimica Industriale,Industriale, via Dodecaneso 31, 16164 Genoa, Italy
[e] Istituto Italiano di Tecnologia, Nanochemistry Department, via Morego 30, 16163 Genova, Italy

ARTICLE INFO

Keywords:
Graphene
Liquid phase exfoliation
Lithium ion battery
Electrodes

ABSTRACT

We unravel the role of flake dimensionality on the lithiation/de-lithiation processes and electrochemical performance of anodes based on few-(FLG) and multi-layer graphene (MLG) flakes prepared by liquid phase exfoliation (LPE) of pristine graphite. The flakes are sorted by lateral size (from 380 to 75 nm) and thickness from 20 (MLG) to 2 nm (FLG) exploiting a sedimentation-based separation in centrifugal field and, finally, deposited onto Cu disks for the realization of four binder-free anodes. The electrochemical results show that decreasing lateral size and thickness leads to an increase of the initial specific capacity from ≈590 to ≈1270mAhg^{-1}. However, an increasing irreversible capacity is also associated to the reduction of flakes' size. We find, in addition, that the preferential Li ions storage by adsorption rather than intercalation in small lateral size (< 100 nm) FLG flakes has a detrimental effect on the average de-lithiation voltage, resulting on low voltage efficiency of these anodes. We believe that the results reported in this work, provide the guidelines for the practical exploitation of graphene-based electrodes.

1. Introduction

Graphene, [1] thanks to its unique physical [2–6] and chemical properties, [3,7] including chemical stability [8] and electrochemical activity, [9] has drawn growing attention for manifold potential applications, ranging from composites, [3] to (opto)electronic. [4,5] In particular, graphene and its derivatives, such as graphene oxide (GO) [10] and reduced graphene oxide (RGO), [11] are considered promising materials in energy-storage applications. [12,13].

In the field of lithium-ion batteries (LIBs), graphene and its derivatives are being extensively explored for the realization of both anodes [14,15] and cathodes. [16,17] So far, RGO has been the most investigated material both for the realization of hybrid anodes, i.e., in combination with electrochemically active materials [12,13,18–23] and as stand-alone material. [24,25] Though, RGO is anything but the ideal anode material. In fact, although it may provide large Li storage capability, it also shows features that would discourage most battery producers. Amongst these, the commonly large irreversible capacity and the voltage hysteresis between lithiation and delithiation are the most serious ones. [12] Being the content of heteroatoms (e.g., O- and H- containing surface groups) and the amount of defects (e.g., micropores, vacancies, etc.) considered possible causes of such behaviour, graphene flakes produced by pristine graphite, i.e. without disrupting its original carbon backbone with aggressive chemical treatments, have recently come into play as possible advanced Li host [26,27].

Graphene nanoplatelets (GNPs) have demonstrated some appealing features for niche applications (e.g., low temperature and high power), [15,18] but no considerable gain in maximum specific capacity with respect to graphite. For what concern graphene, both theoretical and experimental studies have evidenced that Li storage is not thermodynamically favoured in single-layer graphene (SLG), where only low Li occupancy levels can be achieved. [24,26,28,29] This raises a natural question. What about what lies in between? Is there a critical flakes size where both beneficial properties of graphite (e.g. low operating voltage) and graphene (high conductivity and short diffusion paths) are found? Is few-layer graphene (FLG) a good active material for next-generation Li-ion batteries? Despite the fact that it is well accepted that lateral size

* Corresponding authors.
E-mail addresses: stefano.passerini@kit.edu (S. Passerini), francesco.bonaccorso@iit.it (F. Bonaccorso).

http://dx.doi.org/10.1016/j.ssc.2016.12.016
Received 26 November 2016; Accepted 22 December 2016
Available online 23 December 2016

and thickness (i.e. dimensions from now on) of the flakes, [26] as well as their edges, [30] are expected to play key roles on the Li^+ ion storage mechanisms [26,30–33] the link between these morphological properties, and electrochemical performances has not been established yet, neither for RGO, [12,13,19,21–23,25,34–36] nor with the less investigated un-functionalized flakes. [12,13,26,27].

With this work we aim at filling this gap. We exploit an "ad hoc" designed liquid phase exfoliation (LPE) procedure to prepare graphene-based flakes having variable dimensions in terms of dimensions. By means of sedimentation-based separation (SBS) in centrifugal field we obtain a set of FLG and multi-layer graphene (MLG) flake (i.e., FLG < 8 layers and MLG≥8 layers, respectively) [3] dispersions, which are then used to prepare binder-free anodes. The obtained data unravel the influence of the interplay of lateral size (ranging from 75 to 380 nm) and thickness (from 2 to 20 nm, e.g. with the higher end being a thickness comparable with the one of GNPs) of the flakes on the electrochemical performance upon lithiation/de-lithiation. The results indicate that the interplay between increased specific capacity voltage efficiency and irreversible effects make pristine graphene flakes not a promising anode active material in Li-ion batteries.

2. Experimental

The experimental details concerning the samples preparation and spectroscopic/microscopic characterization, as well as electrodes preparation and electrochemical characterization are reported in the supplementary information (S.I.).

3. Results and discussion

3.1. Physical-chemical characterization

We used LPE [37–39] to disperse graphite flakes in N-Methyl-2-Pirrolidone, having a surface tension (41.2 mN m^{-1}) [37–39] close to the graphene surface energy (62 mJ m^{-2}), [40,41] using ultrasonication to exfoliate graphite, see S.I. for details.

The obtained dispersion contains a heterogeneous distribution of thin/thick and small/large lateral size graphitic flakes, [37,39] which are subsequently ultracentrifuged exploiting the SBS process, [26,40,42,43] for the sorting of flakes by dimensions. In order to meet the requirements of fast deposition and non-toxicity, [37,41] the sediment is collected and dispersed in ethanol, allowing the simple one-step fabrication of binder-free electrodes. [27] The electrodes do not contain any additional conductive carbon, largely used in literature, [44] which might interfere with the electrochemical response of the graphene (e.g., by contributing to the Li storage capacity).

The morphology of the samples is characterized by transmission electron microscopy (TEM) and atomic force microscopy (AFM) analyses. The TEM images in Fig. 1a and b show that the average lateral size of the graphitic flakes decreases with the increase of the centrifugal speed, passing from 380 nm to 75 nm, see Table 1. The AFM results shown in Fig. 1c and d, demonstrate that both sample#3 and #4 have a much narrower, with respect to sample#1 and #2, thickness distributions, i.e., centred at 5 nm and 2 nm, respectively (see Table 1). Accordingly, Sample#1 and #2 are mostly formed of thick (20–50 layers) MLG flakes, while Sample#3 is composed of thinner MLG (10–15 layers) and Sample#4 comprised of FLG flakes. As also presented in Table 1, both the surface area (SA) data obtained from Brunauer–Emmett–Teller (BET) measurement and the O/C ratio calculated from XPS analysis (see Fig. S5) clearly demonstrate an increment of their values (SA from 114 ± 11 to 414 ± 41 m^2g^{-1} and O/C ratio from 0.045 to 0.110) passing from Sample#1 to Sample#4, respectively.

The comparison of the Raman spectra of the four as-prepared samples (Fig. 1e) illustrates the evolution of the G, D and 2D peaks, see S.I. about the peaks assignment. The reduction of FWHM(2D) from Sample#1 to Sample#4 indicates a decrease in the thickness of the flakes with the increase of the centrifugal speed. Statistical analysis, see section S2.2, shows that Samples#1, #2 and #3 are composed by MLG, while Sample#4 mostly contains FLGs, in agreement with AFM data. The Raman spectra also show an increase of both D and D′ peaks intensity when passing from Sample #1 to Sample #4, which could be explained assuming an increase of defects. The analysis of I(D)/I(G) as a function both FWHM(G) and Disp(G), see section S2.2, shows that there is no in-plane defect caused during the exfoliation process, and the major contribution to the D peak comes from the sample edges, [45] see S.I. for details.

The graphene dispersions deposited on the Cu substrates are characterized by SEM, see Fig. 1f. The micrographs recorded at low magnification (Fig. S6), and representative for the whole area, testify the homogeneity of the binder-free electrodes, independently from the flake size. Higher magnification images (Fig. 1f) reveal that, as the flake dimension decreases, the electrodes surface becomes more flat and compact, which from one hand could improve the electronic transport amongst the flakes, but, on the other hand, may not be beneficial for the lithium storage capacity and transport.

3.2. Electrochemical investigation

The dimensions of the graphene flakes are expected to play a crucial role on their Li^+ storage characteristics. The voltage profiles of Fig. 2a show that upon the first lithiation process the specific capacity of the electrode increases from 591 mAh g^{-1} to 1267 mAh g^{-1} as the average dimensions of the flake decreases from Sample#1 to Sample#4. However, in the de-lithiation process, Li^+ ions are released only to a certain extent, revealing a significant irreversible capacity, e.g., 40% for Sample#1. As the flakes get smaller in dimensions, more charge is irreversibly consumed in the first cycle, resulting in only 35% coulombic efficiency for Sample#4, see Fig. 2a. This loss may be ascribed to the irreversible electrolyte decomposition process leading to the formation of a solid electrolyte interphase (SEI) on the electrode surface. Variations of flake morphology lead to changes in SA (see Table 1) and edge defect, and thus in turn, of electrode reactivity. [46] In fact, as confirmed by the evident plateau evolving in all samples below 0.9 V, the charge associated to such irreversible process increases with decreasing flake dimensions, and, interestingly, the onset for SEI formation is morphology-dependent too. As the dimension of flakes reduces, the electrolyte decomposition occurs earlier, as testified by an upshift of ~100 mV of the associated plateau (see Fig. S7). Such reduced polarization suggests a catalytic effect of small/thin flakes towards the electrolyte reduction.

From the 2nd cycle onward, the specific capacity of Sample#1 and Sample#2 rapidly stabilizes without considerable fade, setting on values of 341 and 366 mAh g^{-1}, respectively, at the 20th cycle. The higher capacity provided by the smaller/thinner flakes appears to be partially lost upon cycling (see Fig. S8). The flake size has a noticeable influence on the potential window in which the capacity is delivered. During lithiation (Fig. S8a) and de-lithiation (Fig. S8b), Samples#1 and #2 provide stable capacities, mainly delivered at low potentials (i.e., in the 0.005–0.2 V and 0.005–0.25 V range for lithiation and de-lithiation, respectively). As the flakes dimension decreases, larger contributions arise from the more positive potential range instead (0.2–3 V and 0.25–3 V for lithiation and de-lithiation). Such behaviour suggests that adsorption of Li^+ is the mechanism primarily responsible for charge storage in small lateral size FLG flakes, [26,47] whereas, intercalation of Li^+ is the main process occurring in MLG flakes.

In order to get further insights in the Li^+ storage process in FLG- and MLG-based electrodes, a differential capacity analysis (Fig. 2b) is carried out in the 0.005–0.3 V potential range. For Samples#1 and #2 the Li^+ storage process evolves with a series of very sharp peaks, demonstrating fast kinetics and high reversibility. As extensively reported in literature, [32] the voltage peak sequence may here be

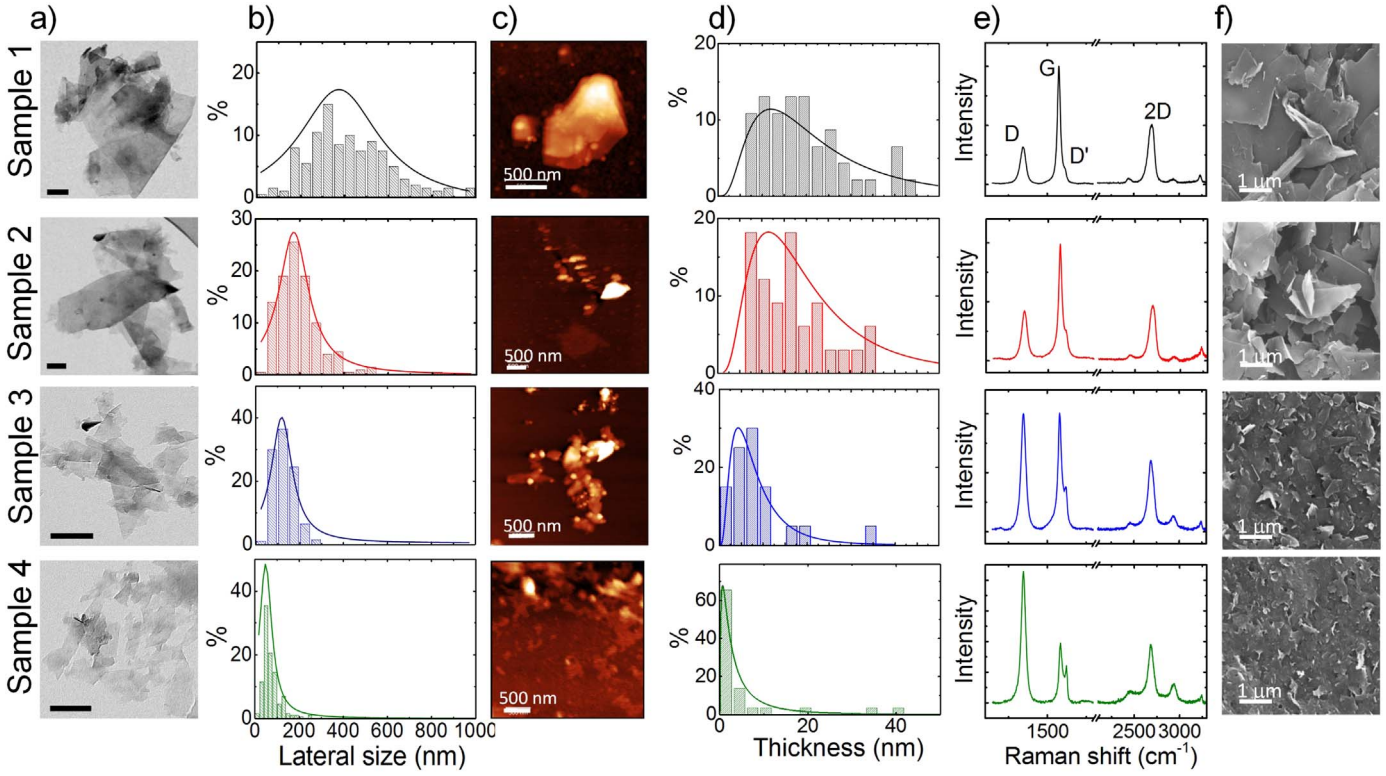

Fig. 1. Morphological analysis of the four samples prepared at different ultracentrifugation speeds, namely 2000 rpm (black, Sample#1), 4000 rpm (red, Sample#2), 10,000 rpm (blue, Sample#3), and 30,000 rpm (green, Sample#4). (a) Representative TEM images and (b) lateral size distribution of flakes (black, Sample#1), (red, Sample#2), (blue, Sample#3), (green, Sample#4) showing a decreasing average distribution with maxima at 380 nm, 180 nm, 120 nm and 75 nm, respectively. The TEM scale bars are 100 nm. (c) Representative AFM images, (d) thickness distribution, and (e) Raman spectra collected at 532 nm excitation wavelength of the four as-produced samples. (f) High resolution SEM images of the four graphene samples deposited onto a Cu substrate. (For interpretation of the references to color in this figure legend, the reader is referred to the web version of this article.)

Table 1
Analysis of the four graphene-based samples prepared in this work at different ultracentrifugation speeds.

	Centrifuge speed (rpm)	Average lateral size (nm)	Average thickness (nm)	Surface area (m^2g^{-1})	O/C ratio
Sample#1	2000	380	20	114 ± 11	0.045
Sample#2	4000	180	10	236 ± 24	0.059
Sample#3	10,000	120	5	317 ± 32	0.085
Sample#4	30,000	75	2	414 ± 41	0.110

explained with the co-existence of phases, similar to those observed for graphite (*four-stage* or *staging mechanism*). [48] From the more diluted phase (> IV) to the fully lithiated one (I), all the main intercalation stages can be clearly detected in Samples#1 and #2. The different stages are still detectable in Sample#3, however with weaker peaks for the IV to III and III to II stage-transitions. The former transition almost vanishes by further reducing the dimension of the flakes, i.e., for Sample#4, suggesting that the majority of the flakes possesses a thickness lower than six layers, as indeed confirmed by the AFM and Raman results. The good news here is that the polarization associated with each intercalation stage, which is a kinetic parameter associated to the energy required to expand the van der Waals gap across two adjacent graphene layers by contrasting the repulsive interactions between guest species, [48] is not affected by the flake size. This is clearly demonstrated, see Fig. 2b, by the fact that the peak positions are, for all samples, matching the values expected on the basis of the related thermodynamic potentials. However, while large and thick flakes (samples#1 and #2) show stable and highly reversible intercalation behaviour, Samples#3 and #4 display a loss of such feature upon the first 20 cycles, which accounts for the aforementioned capacity fading (see Fig. 2a, Fig. S8 and Fig. S10).

Small lateral size MLGs and FLGs would be expected to enable faster Li^+ ions diffusion due to the shorter path lengths for their transport. However, as seen from Fig. 2c, the capacity delivered by Samples#3 and #4 under increasing current load is, already at 0.2 A g^{-1}, inferior to that of Samples#1 and #2 which, on the contrary, provide good capacity retention up to 2 A g^{-1}. Unexpectedly, Sample#3 shows anomalously poor (but reproducible) rate performance, whose cause remains unknown and will be investigated further. After the rate capability test, the electrodes based on Samples#1 and #2 show a full capacity recovery at 0.1 A g^{-1}, with a coulombic efficiency approaching 100%, whereas Samples#3 and #4 show a steeper capacity fading (e.g., only 74% capacity retention for Sample#3). A further contribution to a deeper understanding of the Li^+ storage mechanism of MLG- and FLG-based electrodes is provided by electrochemical impedance spectroscopy (EIS), which shows the typical signature of insertion electrodes (i.e., a redox reaction which involves electrochemical charge transfer (CT) coupled with insertion of guest ions contained in an electrolyte into the physical structure of a solid host). [48] Both SEI and contact resistances are influenced by the flake dimension in a complex manner. Noteworthy, the resistance of the mid-frequency semi-circle (from ca. 6-10 to 0.1 Hz), attributed to the CT of the Li^+ ion uptake process in the FLG- and MLG-based electrodes, displays a significant increase upon the reduction of the flake dimensions, see the Nyquist plot in Fig. S9.

It is evident that changes in dimensions can have great influences on the Li^+ storage capability of FLG and MLG flakes. However, besides looking at the bare capacity values, we should not forget other parameters, which are equally important for practical application in LIBs. As the flakes size decreases, more capacity is delivered at high

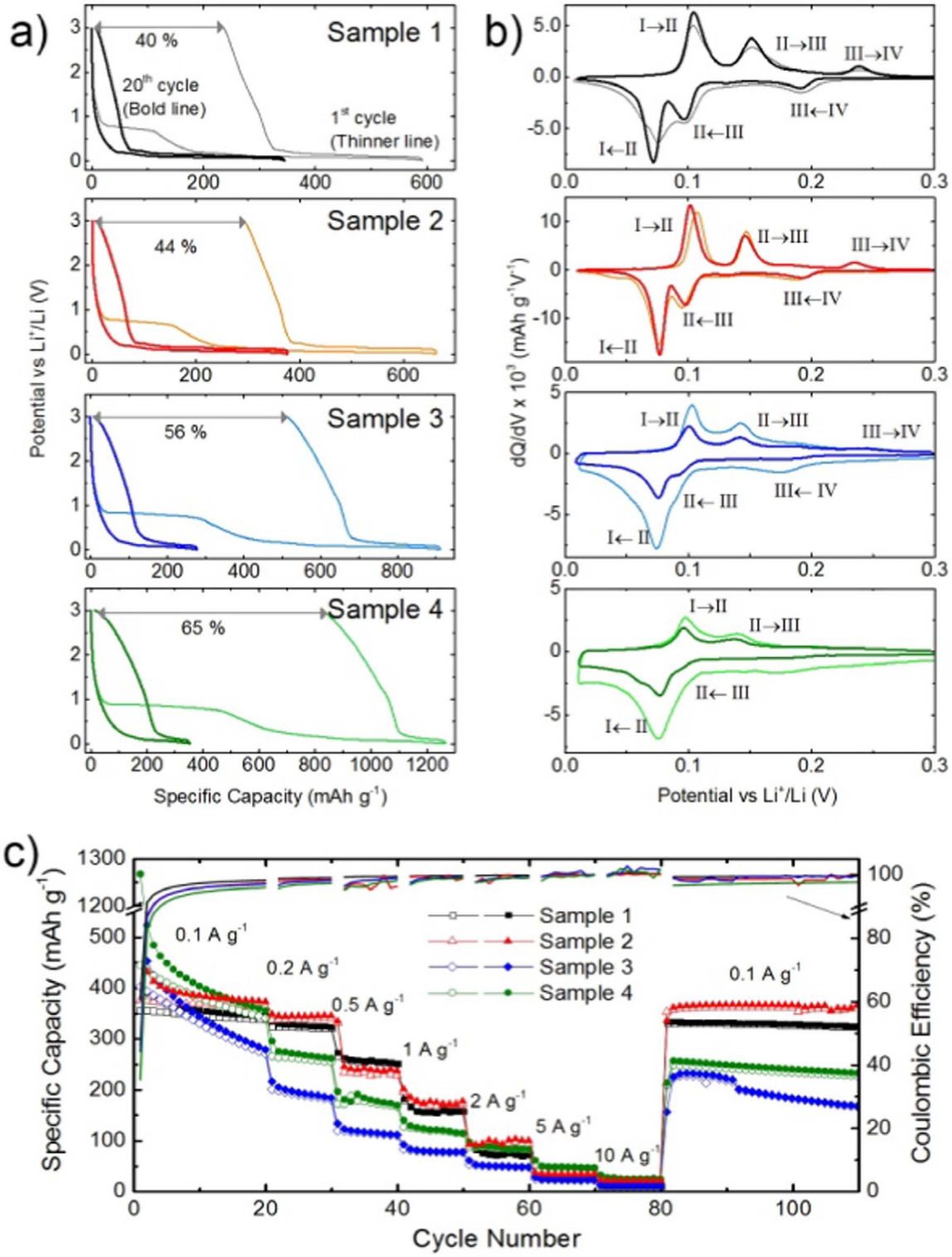

Fig. 2. Electrochemical response of the four graphene-based electrodes in 3-electrode lithium half-cells configuration. (a) Voltage profiles and (b) differential capacity plots for the 1st (dash) and 20th (solid) cycle (current rate: 0.1 Ag^{-1}). (c) Rate capability test.

potentials. As a matter of fact, high lithiation/de-lithiation potential and sloping voltage profiles, however, might result in reduced and non-constant voltage output from the battery. The normalized charge and discharge cycles reported in Fig. 3a and b clearly highlight to which extent the intercalation (< 0.2 and < 0.25 V) and adsorption (> 0.2 and > 0.25 V) storage contribute to the total state of charge (SOC) or depth of discharge (DOD) of the FLG- and MLG-based anodes. As summarized in Fig. 3c, the intercalation is predominant in large and thick flakes, while it becomes less evident in the smaller and thinner ones. The contribution of adsorption in small and thin flakes is particularly relevant during Li^+ extraction, where it can account for up to 65% of the whole delivered capacity (i.e., in Sample#4).

Such discrepancy between charge and discharge gives rise to a voltage hysteresis, common for carbonaceous materials. [49,50] As reported in Fig. 3d, the higher de-lithiation potentials, associated with the reduction in dimensions of the flakes, do increase considerably the

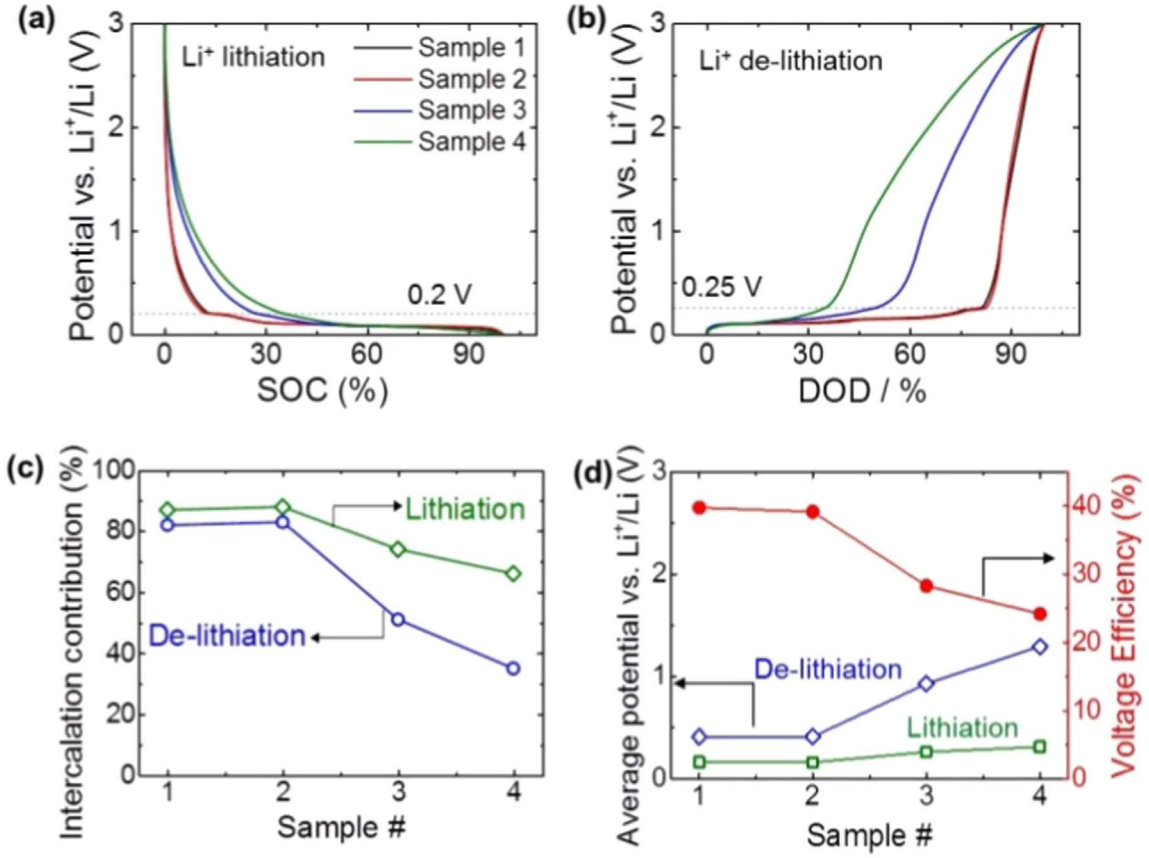

Fig. 3. Normalized voltage profiles of the four graphene-based samples in terms of (a) SOC and (b) DOD (obtained from the 20th cycle at 0.1 A g^{-1}). (c) Contribution of the intercalation mechanism to the total charge (calculated as the percentage of charge stored below 0.2 V or delivered above 0.25 V for lithiation and de-lithiation, respectively). (d) Effect of lithiation and de-lithiation average potentials on the voltage efficiency of the graphene anodes (the average potentials are obtained by the integral of the voltage profiles divided by the specific gravimetric capacity. The voltage efficiency is calculated as the ratio between de-lithiation and lithiation average potentials).

electrode average voltage during discharge. This has a detrimental effect on the voltage efficiency which, ultimately, is reduced from 40% (of Sample#1 and #2) to 25% (Sample#4).

4. Conclusion

In this work, we report a systematic and comprehensive study on the role of the morphology of multi- to few-layer graphene flakes on their electrochemical properties as anode for lithium-ion batteries. The results demonstrate that changes in the flakes dimensions have indeed a massive impact into their capability of storing Li^+ ions.

The reduction of flake lateral size/thickness does enable higher specific capacity values in the first cycle. However, the amount of charge loss associated with the formation of solid electrolyte interface dramatically increases. Smaller flakes also show slower charge transfer kinetics attributable to lower Li-to-C binding energies and stronger coulombic repulsion among Li^+ ions, with respect to the larger counterparts. Interestingly, the staging behaviour of graphite, typical "fingerprint" of the intercalation mechanism, is always observed in all samples. However, as the flake dimensions are reduced, the intercalation mechanism appears to become less reversible. Whether this phenomenon arises from surface passivation, trapping of Li^+ ions, or other effects is still unclear being object of further investigations. Furthermore, a larger contribution of Li^+ adsorption to the overall storage capacity can be clearly noticed passing from multi-layer to few-layer graphene flakes. This has a detrimental effect on the average de-lithiation voltage, which substantially increases with decreasing the flake dimension, resulting on lower voltage efficiency with respect to anodes based on multi-layer graphene.

In summary, we demonstrated that the quest for the ultimate anode material for lithium-ion batteries is still open. Graphene might be involved in it, but, surely not as the main character. Anodes composed entirely either of graphene or graphene oxide/reduced graphene oxide are probably not suited for the task. Certainly, issues like the initial capacity loss may be "easily" addressable, e.g., by pre-lithiation. [26] On the other hand, to maximize the energy output of lithium-ion batteries, an anode material should release Li^+ ions at lower potentials. With regard to this last point, at this stage, silicon is a more appealing candidate than graphene.

Acknowledgements

This work was supported by the European Commission through the Graphene Flagship – Core 1 project (GA-696656).

Appendix A. Supplementary material

Supplementary data associated with this article can be found in the online version at doi:10.1016/j.ssc.2016.12.016.

References

[1] K.S. Novoselov, A.K. Geim, S.V. Morozov, D. Jiang, Y. Zhang, S.V. Dubonos, I.V. Grigorieva, A.A. Firsov, Science 306 (2004) 666–669.
[2] A.K. Geim, K.S. Novoselov, Nat. Mater. 6 (2007) 183–191.
[3] A.C. Ferrari, et al., Nanoscale 7 (2015) 4598–4810.
[4] F. Bonaccorso, Z. Sun, T. Hasan, A.C. Ferrari, Nat. Photonics 4 (2010) 611–622.
[5] G. Fiori, F. Bonaccorso, G. Iannaccone, T. Palacios, D. Neumaier, A. Seabaugh, S.K. Banerjee, L. Colombo, Nat. Nanotechnol. 9 (2014) 768–779.

[6] M.D. Stoller, S. Park, Y. Zhu, J. An, R.S. Ruoff, Nano Lett. 8 (2008) 3498–3502.
[7] S. Park, R.S. Ruoff, Nat. Nanotechnol. 4 (2009) 217–224.
[8] J.S. Qi, J.Y. Huang, J. Feng, D.N. Shi, J. Li, ACS Nano 5 (2011) 3475–3482.
[9] Y. Shao, J. Wang, H. Wu, J. Liu, I.A. Aksay, Y. Lin, Electroanalysis 22 (2010) 1027–1036.
[10] D.R. Dreyer, S. Park, C.W. Bielawski, R.S. Ruoff, Chem. Soc. Rev. 39 (2010) 228–240.
[11] S. Stankovich, D.A. Dikin, R.D. Piner, K.A. Kohlhaas, A. Kleinhammes, Y. Jia, Y. Wu, S.T. Nguyen, R.S. Ruoff, Carbon 45 (2007) 1558–1565.
[12] R. Raccichini, A. Varzi, S. Passerini, B. Scrosati, Nat. Mater. 14 (2014) 271–279.
[13] F. Bonaccorso, L. Colombo, G. Yu, M. Stoller, V. Tozzini, A.C. Ferrari, R.S. Ruoff, V. Pellegrini, Science 347 (2015) (1246501–1246501).
[14] P.G. Bruce, B. Scrosati, J.-M. Tarascon, Angew. Chem. Int. Ed. 47 (2008) 2930–2946.
[15] R. Raccichini, A. Varzi, V.S.K. Chakravadhanula, C. Kübel, A. Balducci, S. Passerini, J. Power Sources 281 (2015) 318–325.
[16] B. Lung-Hao, Hu, F.-Y. Wu, C.-T. Lin, A.N. Khlobystov, L.-J. Li, Nature Commun. 4 (2013) 1687.
[17] J.B. Goodenough, J. Power Sources 174 (2007) 996–1000.
[18] R. Raccichini, A. Varzi, V.S.K. Chakravadhanula, C. Kübel, S. Passerini, Sci. Rep. 6 (2016) 23585.
[19] K. Evanoff, A. Magasinski, J. Yang, G. Yushin, Adv. Energy Mater. 1 (2011) 495–498.
[20] L. Ji, M. Rao, H. Zheng, L. Zhang, Y. Li, W. Duan, J. Guo, E.J. Cairns, Y. Zhang, J. Am. Chem. Soc. 133 (2011) 18522–18525.
[21] S.-L. Chou, J.-Z. Wang, M. Choucair, H.-K. Liu, J.A. Stride, S.-X. Dou, Electrochem. Commun. 12 (2010) 303–306.
[22] Z.-S. Wu, W. Ren, L. Wen, L. Gao, J. Zhao, Z. Chen, G. Zhou, F. Li, H.-M. Cheng, ACS Nano 4 (2010) 3187–3194.
[23] Y. Shi, J.-Z. Wang, S.-L. Chou, D. Wexler, H.-J. Li, K. Ozawa, H.-K. Liu, Y.-P. Wu, Nano Lett. 13 (2013) 4715–4720.
[24] E. Yoo, J. Kim, E. Hosono, H.-s. Zhou, T. Kudo, I. Honma, Nano Lett. 8 (2008) 2277–2282.
[25] D. Wang, et al., ACS Nano 3 (2009) 907–914.
[26] J. Hassoun, et al., Nano Lett. 14 (2014) 4901–4906.
[27] H. Sun, et al., J. Mater. Chem. A 4 (2016) 6886–6895.
[28] E. Pollak, B. Geng, K. Jeon, I.T. Lucas, T.J. Richardson, F. Wang, R. Kostecki, Nano Lett. 10 (2010).
[29] M. Liang, L. Zhi, J. Mater. Chem. 19 (2009) 5871.
[30] C. Uthaisar, V. Barone, Nano Lett. 10 (2010) 2838–2842.
[31] G. Wang, X. Shen, J. Yao, J. Park, Carbon 47 (2009) 2049–2053.
[32] P. Roy, S.K. Srivastava, J. Mater. Chem. A 3 (2015) 2454–2484.
[33] S. Goriparti, E. Miele, F. De Angelis, E. Di Fabrizio, R. Proietti Zaccaria, C. Capiglia, J. Power Sources 257 (2014) 421–443.
[34] R. Hu, W. Sun, Y. Chen, M. Zeng, M. Zhu, J. Mater. Chem. A 2 (2014) 9118.
[35] G. Zhou, D.-W. Wang, F. Li, L. Zhang, N. Li, Z.-S. Wu, L. Wen, G.Q. Lu, H.-M. Cheng, Chem. Mater. 22 (2010) 5306–5313.
[36] O.A. Vargas C, Á. Caballero, J. Morales, Nanoscale 4 (2012) 2083.
[37] F. Bonaccorso, A. Lombardo, T. Hasan, Z. Sun, L. Colombo, A.C. Ferrari, Mater. Today 15 (2012) 564–589.
[38] K.R. Paton, et al., Nat. Mater. 13 (2014) 624–630.
[39] F. Bonaccorso, A. Bartolotta, J.N. Coleman, C. Backes, Adv. Mater. 28 (**2016**) 6136–6166.
[40] Y. Hernandez, et al., Nat. Nanotechnol. 3 (2008) 563–568.
[41] A. Capasso, A.E. Del Rio Castillo, H. Sun, A. Ansaldo, V. Pellegrini, F. Bonaccorso, Solid State Commun. 224 (2015) 53–63.
[42] F. Torrisi, et al., ACS Nano 6 (2012) 2992–3006.
[43] O.M. Maragó, et al., ACS Nano 4 (2010) 7515–7523.
[44] M. Yoshio, R.J. Brodd, A. Kozawa, Lithium-Ion Batteries, Springer, 2009.
[45] A.C. Ferrari, D.M. Basko, Nat. Nanotechnol. 8 (2013) 235–246.
[46] D. Pan, S. Wang, B. Zhao, M. Wu, H. Zhang, Y. Wang, Z. Jiao, Chem. Mater. 21 (2009) 3136–3142.
[47] H.F. Xiang, Z.D. Li, K. Xie, J.Z. Jiang, J.J. Chen, P.C. Lian, J.S. Wu, Y. Yu, H.H. Wang, RSC Adv. 2 (2012) 6792.
[48] M. Winter, J.O. Besenhard, M.E. Spahr, P. Novák, Adv. Mater. 10 (1998) 725–763.
[49] N.A. Kaskhedikar, J. Maier, Adv. Mater. 21 (2009) 2664–2680.
[50] C. de las Casas, W. Li, J. Power Sources 208 (2012) 74–85.